General circulation and intergyre dynamics in the eastern North Atlantic from a regional primitive equation model

Thierry Penduff, Alain Colin de Verdiere, Bernard Barnier

Journal of Geophysical Research, 106, pp 22,313-22,329, 2001.

General circulation and intergyre dynamics in the eastern North Atlantic from a regional primitive equation model

Thierry Penduff
Laboratoire des Ecoulements Géophysiques et Industriels, Grenoble, France

Alain Colin de Verdière
Laboratoire de Physique des Océans, Université de Bretagne Occidentale, Brest, France

Bernard Barnier
Laboratoire des Ecoulements Géophysiques et Industriels, Grenoble, France

Abstract

The mean circulation of the eastern North Atlantic is investigated using a regional $0.8° \times \cos(\text{latitude})$-resolution configuration of the SPEM primitive equation sigma coordinate model, forced by seasonal and monthly surface fluxes. The computational domain is surrounded by three self-adapting open boundaries which evacuate the outgoing perturbations and laterally control the baroclinic modes in inflow regions, but let the model adjust the barotropic mode to a large extent. The final solution is stable and reproduces most features of the basin's mean circulation well: A realistic Azores Current, the observed paths and transports of subpolar currents, of the branches of the North Atlantic Current, of the intergyre zone modal and intermediate water masses down to about 2000 m. A few unrealistic circulation features, attributed to the modest resolution and to certain limitations of the sigma coordinates, are found below 2000 m. The buoyancy and vorticity balances are investigated in the intergyre zone. The Subpolar Mode Water (SPMW), subducted at a realistic rate, continues its southward journey toward the ocean's interior in accordance with the ventilated thermocline theory, with eddy diapycnal fluxes exerting a moderating effect. The poleward motion of the Mediterranean Water (MW) is reproduced well north of 45°N and governed by similar dynamics, but is absent south of 45°N. The southward motion of Labrador Sea Water (LSW) is mainly driven by diapycnal fluxes induced by vertical diffusion, which exert vertical stretching. This explanation contrasts with a recent study where salt fingering was shown to drive a similar LSW circulation.

1. Introduction

The mean circulation and dynamics of the North Atlantic Ocean are better known west of the Mid-Atlantic Ridge (MAR) than east of it. This situation has historical origins but still persists, probably because the ocean dynamics differ between the two basins. In the western basin, the mean flow is dominated by the Gulf Stream extension, a permanent, intense and thin (about 100 km-wide) jet that remains confined within a rather limited area (about 2°-wide, *Kelly* [1991]). East of 45°W the major current (North Atlantic Current, NAC) is weaker and splits into several branches whose number, intensity, T-S structure and path are subject to intense interannual variability [*Sy et al.,* 1992]. Other major features of the mean circulation in the eastern basin, such as the warm water export toward the Norwegian Sea [*Orvik et al.,* 1999], its return flow above the Greenland-Iceland-Scotland sills [*Bacon,* 1998], or the current regime between the subpolar and the subtropical gyres [*Sy,* 1988] are linked with the NAC and also exhibit an important interannual variability.

Present estimates of the large-scale circulation in the basin are thus restricted to given periods, areas or immersions: The early eighties [*Sy,* 1988; *Arhan et al.,* 1989; *Sy et al,* 1992; *Gana and Provost,* 1993], the late winter in the eighties [*Paillet and Mercier,* 1997] (noted PM97 thereafter), the near-surface mean circulation during the eighties [*Brügge,* 1995] or the early nineties [*Otto and van Aken,* 1996]. *Schmitz and McCartney* [1993] proposed a synthesis of numerous local measurements and schemes of the North Atlantic mean circulation, but pointed out that "there are still significant gaps in our knowledge of [this] circulation".

Among available in situ measurements, hydrographic data are probably the most abundant east of the MAR and constitute an interesting starting point to evaluate the mean circulation. However, hydrography-based direct estimates of transports across individual sections may not accurately represent the dynamical impact of topography on the large-scale flow, shown to be crucial at these latitudes [*Wunsch and Roemmich,* 1985; *Arhan et al.,* 1989], because a level of no motion has to be chosen. This choice is partly arbitrary, has a significant impact on the total transport [*Paillet and Mercier,* 1997], and certainly distorts the topographic effect. In addition to the interannual variability, this explains why geostrophic estimates of the NAC transport above the MAR cover a wide range (see Table 2 in *Sy et al* [1992]). North of about 40°N, geostrophic estimates of the current transports should thus be interpreted with caution.

One may also deduce the mean flow in the basin from a set of dynamical equations and a T-S annual climatology based on several decades of hydrographic data. A mean velocity field representative of these decades may be computed from such a stratification by an inverse model (as was done for one particular season by PM97), but the possible mean contribution of the wind- and buoyancy-driven variability cannot be addressed. Our approach is to initialize a prognostic non-eddy-resolving primitive equation model of the basin with a climatological T-S stratification representative of a given season, and to integrate the model with a realistic seasonal forcing until stabilization. The final mean stratification and circulation are thus adjusted mutually and to the surface forcing, and explicitly integrate the ocean variability up to seasonal timescales. Provided that the model and its surface forcings are reliable, and that the spinup leads to a realistic and stable solution, this prognostic approach helps to complete in situ or inverse estimates of the mean circulation. This is the first aim of the present study.

Our second goal is to investigate the origin of subsurface currents in the so-called intergyre region, located between the NAC and the Azores Current (AC). The ventilated thermocline theory [*Luyten et al,* 1983] provides an explanation of the way in which layers lying below a directly wind-driven surface layer can be put into motion: In regions of downward Ekman pumping, fluid columns can be subducted beneath the surface layer and continue their southward journey conserving their low potential vorticity acquired at outcrop lines. An important result of this adiabatic calculation was the appearance of shadow zones along eastern boundaries, which occur due to the strict adherence to the conditions of potential vorticity conservation and zero normal geostrophic velocity at the eastern boundary. Another way of putting deep layers in motion is through internal turbulent diffusion. *Luyten and Stommel* [1986] describe case studies in which solutions appropriate to the subtropical gyre heating, subpolar gyre cooling, and wind stress distributions are obtained through Sverdrup dynamics. Although the surface stress distribution can be considered as given, it is another matter for the heating-cooling distributions that are closely interrelated with the large-scale advection field one wishes to calculate. An alternative to the arbitrary distribution of their cross-isopycnal flux is to "observe" the links between

the large-scale circulation and the turbulent forcing fields in a numerical model, and to interpret those links at the level of Sverdrup dynamics. For this to be a fruitful exercise, the model solution should be close to the real circulation so that the motions of known water masses can be associated with different contributions to the stretching term in the planetary vorticity equation. Once our eastern North Atlantic model produces realistic flow rates for the water masses, we shall investigate how the three major water masses of the basin (Subpolar Mode Water, Mediterranean Water and Labrador Sea Water) are set in motion.

To date, the results of several North Atlantic models have been published and a number of comparisons made [*Schott and Böning,* 1991; *DYNAMO Group,* 1997]. These comparisons reveal significant differences and discrepancies east of the MAR (distorted and weak NAC, absence of the AC), even at high resolution. These weaknesses may be linked to the inability of most basin-scale models to reproduce the Gulf Stream separation process properly. Our numerical domain was thus restricted to the eastern basin through the use of "self-adapting" open boundaries [*Penduff et al.,* 2000] (noted P00 hereafter), partly controlled by recent climatological T-S fields.

The paper is divided into several sections. In section 2, we briefly summarize the model configuration. In section 3, the final mean circulation is described and compared with available estimates. The impact of internal diffusive processes on the motion of the water masses in the intergyre zone is investigated in section 4. Our results are summarized in section 5.

2. Model Configuration

The present study is conducted using the SPEM5.1 primitive equation model at a resolution of 0.8° in longitude and $0.8° \times \cos(\phi)$ in latitude ϕ. The limits of the study area are justified in P00 and shown in Figure 1. SPEM uses sigma coordinates on the vertical, which allow a more natural treatment of the bottom topography condition. The possible tendency of geopotential coordinate models to overestimate the blocking effect of the MAR [*Treguier,* 1992] is also avoided with this approach. In order to limit the spurious velocities generated by truncation errors in the pressure gradient calculation, the topography was smoothed using the criterion adopted by *Barnier et al.* [1998] and validated in a "resting stratification case" (see the latter paper). The actual topography used in our simulations is depicted in Figure 2 and leads to erroneous velocities smaller than 0.25 cm s^{-1} over most of the domain. The regions where numerical errors induce unrealistic features are pointed out in section 3.

Along the western (40°W), southern (30°N) and eastern (0.8°W) limits, original self-adapting open boundaries (OBs) evacuate the outgoing perturbations through radiation equations, and, in inflow regions, constrain the interior circulation by a strong relaxation of the baroclinic variables to a seasonal climatology. This lateral baroclinic climatology and the initial stratification come from the recent T-S climatology of *Reynaud et al.* [1998] (noted RLM hereafter). These fields are based on several decades of hydrographic data and exhibit marked horizontal density gradients, thus providing the main incoming currents with a realistic location and baroclinic structure (especially along 40°W). Along these three OBs, the vertically-integrated flow (hereafter referred to as "barotropic" and denoted ψ), and consequently a large part of the lateral dynamical forcing, is adjusted to the interior dynamics by the model itself. This novel degree of freedom is a key element in our simulations. During model integration, along the northern "fixed" boundaries of the domain (66.5°N), the temperature, salinity, and baroclinic velocity fields were kept equal to their RLM climatological seasonal estimates, and the barotropic stream function was prescribed to a linear profile between Greenland, Iceland and the northeastern corner. The reader is referred to P00 for a detailed description of the lateral forcing and of its impact on the interior solution. Table 1 and Table 2 summarize the parameters involved in this lateral forcing. The other model parameters, the surface buoyancy and mechanical forcings are presented in Table 3.

Table 1

Table 2

Table 3

3. Annual Mean Circulation

P00 present the dynamical and thermodynamical adjustment of the basin, and show that the annually-averaged solution totally stabilizes after 35 years of integration. This is remarkable in the presence of such extensive self-adapting open boundaries. A scheme of the model mean circulation after 38 years of integration is shown in Figure 3 for three layers. The horizontal transports of individual currents indicated in this figure were computed across several zonal and meridional sections; the vertical transports were then deduced from the divergence of horizontal mass fluxes between these sections to close the mass budget. Fig-

Figure 3

ure 4 presents the annually- and depth-averaged flow (ψ).

3.1. The North Atlantic Current and the Subpolar Gyre

The NAC enters the domain between 43°N and 51°N and brings more than 40 Sv (depth integral) above the MAR into the eastern basin; most of this transport (29.8 Sv) is confined to the upper 800 m (Figure 3a). The barotropic flow (Figure 4) is significantly different from the Sverdrup transport (Figure 5), suggesting that only two thirds of the NAC transport can be forced by the wind stress curl alone. Indeed, all along the modeled NAC and throughout the water column (Figures 3a, 3b), large-scale downwelling strengthens the northward component of the flow through vortex stretching and consequently increases the transport above the MAR. This interaction between topographic slopes and bottom currents was shown to be of major importance for mid-latitude dynamics by *Wunsch and Roemmich* [1985] and *Arhan et al.* [1989]. In the inverse model of PM97 and in the present simulation, the NAC transport is increased by 30% through this topographic effect.

Our estimate of the NAC transport above the MAR, like the inverse estimates of *Gana and Provost* [1993] and PM97 (48 and 58 Sv respectively), significantly exceeds hydrography-based geostrophic estimates, which range between 16 Sv [*Wegner,* 1973] and 32 Sv [*Krauss et al.,* 1987]. Indeed, inverse and prognostic models represent the interaction of bottom currents with the topographic slopes, a process which is distorted or neglected in geostrophic computations when assuming the existence of a reference level at depth.

Figure 3 shows that the NAC is deflected northeastward at all depths above the MAR, as suggested by *Sy* [1988] (his figure 11), but more markedly than in certain other studies [PM97; *Otto and Van Aken,* 1996]. This steering is associated with a local maximum of the vertical stretching within the Charlie Gibbs Fracture Zone (CGFZ), where the bottom flow is downslope and eastward. The westward bottom flow observed in this passage [*Saunders,* 1994] is not reproduced by the model probably because the local vertical resolution (about 500 m near the bottom) is too weak for a correct representation of the vertical shear of horizontal velocities. Downstream of the MAR, two thirds of the NAC transport circulates northward, as proposed by the inverse model of PM97. The NAC spreads into several branches, two of which feed the subpolar gyre:

1. A 24.1-Sv branch, which has a strong vertical shear (70% of its transport is confined to the upper 800 m, Figure 3a) and enters the eastern basin between 49°N and 54°N. Its upper part (above 1500 m) brings 16.8 Sv northward between the Rockall Plateau and Scotland (close to the 14-Sv estimate of *McCartney and Talley* [1984]). About 11 Sv of this warm Atlantic water enter the Norwegian Sea above the Iceland-Scotland Ridge (ISR) in two branches of similar intensity (5.6 and 5.7 Sv, Figure 3a). This total surface outflow is about 30% stronger than the estimate of *Orvik et al.* [1999].

2. The northernmost branch of the NAC brings 12.2 Sv from the MAR toward the eastern Iceland Basin. This branch is vertically more coherent since about 55% of its transport (6.8 Sv, Figure 3a) is found above 800 m.

The westward transport of Iceland-Scotland Overflow Water (ISOW, $\sigma_0 > 27.8$) above the ISR sill was estimated to be 2.7 Sv by *Dickson and Brown* [1994]. In the model, this transport depends on the section considered, since a strong entrainment exists in this area, and ranges between 2.3 Sv and 3.5 Sv. As in the circulation scheme proposed by these authors, the model ISOW then spreads into the Rockall Trough and along the ISR western flank, recirculating mainly within the subpolar gyre. The depth-integrated westward transport south of Iceland reaches about 21 Sv (31 Sv for *Schmitz and McCartney* [1993]).

The Irminger Current enters the model domain by the western boundary near 60°N; its depth-averaged transport is then 7 Sv with a significant contribution from all layers (Figure 3). It is later augmented by the contribution of a branch from the northern NAC which does not enter the eastern basin. This increases the northward transport to 12.7 Sv west of the Reykjanes Ridge. The Irminger Current circulates cyclonically and meets the East Greenland Current (EGC). The 9-Sv southward flow prescribed through the Denmark Strait finally intensifies the EGC transport up to 41.8 Sv. This value was not constrained a priori, but is similar to *Schmitz and McCartney* [1993]'s estimate. The model solution in the subpolar gyre is also very close to the circulation scheme of *Otto and van Aken* [1996], derived from drifter data.

3.2. The Intergyre Zone and the Subtropical Gyre

East of the MAR, the southward-recirculating branches of the NAC bring more than 11 Sv of water (distributed over the three layers of Figure 3) toward the subtropical gyre across the intergyre zone. Like the PM97 circulation scheme, our solution above 800 m shows the southern limit of the subpolar gyre to lie largely south (around 47°N) of what would be expected without topographic forcing (i.e., the zero contour in Figure 5). Between 40°N and 50°N, about 1.75 Sv of Subpolar Mode Water (SPMW) are subducted into the ocean thermocline [*Penduff,* 1998]; with the same method, PM97 obtain a similar subduction rate (2.5 Sv).

The subtropical gyre is also fed from the west above 800 m by the Azores Current (AC), rarely simulated by coarse-resolution models. The AC brings 9.2 Sv eastward across 35°W between 30°N and 35°N, is fed from the north all along its eastward path by the southward flow of thermocline waters (4.5 Sv), and loses 8.3 Sv southward between the MAR and 20°W (Figure 3a). The AC intensity thus decreases downstream, and only 4.4 Sv leave the domain through the southern boundary east of 20°W. These features are remarkably coherent with the results of *Stramma* [1984] and *Klein and Siedler* [1989], and with the circulation scheme of *Siedler and Onken* [1996] (their figure 11.6).

At intermediate levels, a cyclonic circulation surrounds the Mediterranean Water (MW) tongue (Figure 3b). A similar tendency is described by *Reid* [1994], and deduced by *Schmitz and McCartney* [1993] with a level of no motion below the MW (as in the present solution, see section 4). However, results from *Saunders* [1982] and *Maillard* [1986] contradict this picture. Within the MW, north of about 35°N, these authors report a poleward flow which was rationalized by *Schopp and Arhan* [1986]. This latter point of view appears more convincing to us; we will come back to this deficiency of the model in the next section.

At a depth of about 1750 m, the Labrador Sea Water (LSW) crosses the MAR within the NAC system and splits into three main branches (Figure 3c): A northeastward flowing vein joins the subpolar gyre; a second branch follows the eastern flank of the MAR southward with local recirculations toward the western basin, and finally flows around the Azores Plateau; the third branch goes across the eastern basin, steers southeastward and passes to the south of the Azores. However, the model concentrates this third branch along the Porcupine Bank north of 48°N. This feature appears unrealistic and due to the use of sigma coordinates since it is also observed in the resting stratification case. *Knochel* [1998] reports a similar tendency in a coarse-grid North Atlantic configuration of SPEM; his results suggest that a significant increase (almost double) in the vertical resolution would correct this discrepancy. Except for this feature, the LSW general circulation in the model closely agrees with the circulation schemes of *Paillet et al.* [1998] and *Speer et al.* [1999]; the southward transport of LSW east of the MAR (2.9 Sv across 44°N) is similar to Paillet et al.'s estimate.

Below 2000 m in the subtropical gyre, the model drives a 3.5 Sv to 8.8 Sv deep anticyclonic circulation. It is depicted by the dark loop in Figure 3c, and has a signature on ψ along the coast of Europe (Figure 4). This circulation is opposite to that observed by *Dickson et al.* [1985], and may be due to the use of sigma coordinates since a southward flow along the coast of Portugal is also visible in the resting stratification case, and in coarse- and fine-grid North Atlantic configurations of SPEM [*Knochel,* 1998; *DYNAMO Group,* 1997]. In the present regional configuration in particular, this discrepancy at depth can hardly be compensated for by either the largely passive self-adapting southern open boundary or the surface forcing which mainly affects the layers located above the marked thermocline.

3.3. Zonally-Averaged Circulation in the Intergyre Zone

By way of an introduction to section 4, the zonally- and annually-averaged model meridional velocity field is presented at different latitudes in Figure 6. Below the ageostrophic surface Ekman layer, this figure may be compared with the zonally-averaged absolute geostrophic velocity field estimated from hydrography by *Saunders* [1982] (Figure 6b) at the same latitudes, under the assumption of a Sverdrupian barotropic flow. Since the geostrophic balance and the Sverdrupian nature of the depth-integrated flow may be affected by ageostrophic currents and topographic effects along the eastern boundary, and since the model results exhibit a few discrepancies along the coast, we chose a band of zonal averaging (24°W-16°W) narrower than that considered by Saunders (from the MAR to the eastern boundary). Our estimate is still representative of the large-scale circulation in the eastern basin and is close to the estimate by Saunders,

as shown below.

Between 48°N and 30°N, the southward advection of Central Waters and SPMW by the NAC is well simulated within a surface layer that thickens southward (from 300 to 800 m). North of 45°N, below this surface current, denser SPMW flows northward within a layer that thickens progressively, as estimated by Saunders.

Around 1000 m within the tongue of MW, the model meridional flow is weak at all latitudes; it is oriented southward at 36°N and 41.5°N and northward north of about 45°N. Saunders reports a poleward flow at this depth, but also within the band 36°N-45°N. This model discrepancy may be related to the crude representation of the MW overflow in the Gulf of Cadiz. The parametrization of the MW source term by a simple T-S relaxation, the presence of a closed boundary at the strait, the absence of important topographic details and steep slopes in the smoothed bathymetry, and the modest horizontal resolution are likely to distort the local dynamics (in particular, the absence of the observed northward flowing MW vein along the coast of Portugal) and the large-scale solution within the MW intrusion. Another explanation will be proposed below.

Between 1000 and 2000 m, the model reproduces the southward flow of LSW mentioned by Saunders and *Paillet et al.* [1998] between 35°N and 46°N, with a maximum velocity near 37°N. This feature will appear more clearly in section 4.

The northward flow visible below 2000 m in Figure 6a corresponds to the western part of the deep basin-wide anticyclone mentioned earlier (Figure 3c). Contrary to what Figure 6a suggests, this unrealistic model feature does not induce any net meridional transport in the deep eastern basin, since the region of the European shelf, along which the southward return flow is confined, is excluded from the band of longitudinal averaging.

3.4. Summary

The discrepancies in the model are found at the following locations: in the CGFZ, where the observed westward bottom flow is not simulated and where the NAC northward deflection may be overestimated (these features are probably related); around the Porcupine Bank, where numerical effects slightly confine the LSW southward flow; below 2000 m in the deep subtropical basin, where the model generates an unrealistic anticyclonic flow; in the southern part of the MW intrusion, where the observed northward flow is not simulated.

However, the current paths and intensities are in good agreement with available direct estimates over most of the basin, without any local constraint on the barotropic stream function at the open boundaries. P00 showed that the model solution is also robust, since it is insensitive to the net mass exchange prescribed between the basin and the rest of the Atlantic. This suggests that the model circulation in the eastern basin is largely influenced by the interior forcing. In particular, the strength and the path of the AC and the NAC are not the result of direct forcing at the boundaries, but are driven from the inside of the domain: The geostrophic adjustment to the initial stratification and wind forcing (which induces a meridionally divergent circulation) instantaneously create eastward currents within the domain and across 40°W. These currents are then maintained throughout the integration at the western open boundary by a strong relaxation of their baroclinic structure to the RLM climatology, while the interior dynamics adjust their barotropic transport at each time step.

The model large-scale meridional circulation averaged over the central eastern basin is comparable to the estimates of *Saunders* [1982] above 2000 m; the origin of these currents is investigated in the next section. Additional diagnostics and dynamical investigations (impact of wind forcing, topography, and stratification on ψ, estimation of the SPMW subduction rate, topographic sensitivity experiments) may be found in *Penduff* [1998].

4. Internal Dynamics and Thermodyna- mics of the Intergyre Zone

In the last section, the water mass flow rates in the band 24°W-16°W were shown to be quite realistic above 2000 m in the intergyre region. This mean circulation is now investigated within four potential density layers (Table 4) which are representative of the main water masses. The mean density field is shown in Figure 7. The isopycnal surfaces 26.9, 27.1, and 27.4 lie respectively above, along and below the potential vorticity minimum associated with the core of SPMW. The isopycnal surfaces 27.6 and 27.8 lie approximately below the MW and the LSW, respectively.

Table 4

Figure 7

In a non-diffusive adiabatic ocean, diapycnal ve-

locities are zero and the flow is parallel to isopycnal surfaces. This hypothesis underlies the theory of the ventilated thermocline [*Luyten et al.,* 1983] which has often been used to investigate the large-scale dynamics of this particular region [*Schopp and Arhan,* 1986; *Paillet and Arhan,* 1996]. However, in the real ocean, turbulent diffusion (parameterized in our model by laplacian operators in the vertical and the horizontal) is expected to induce mass exchanges between density layers, and may generate meridional motions in these layers through vortex stretching. Our computations concerning both processes are explained in section 4.1; the dynamical impact of vertical and horizontal diffusion is presented in section 4.2; the importance of diapycnal transfers with respect to the adiabatic part of the flow is discussed in section 4.3.

4.1. Diagnostics

4.1.1. The buoyancy balance. The density equation may be written as follows (subscripts t and z denote the temporal and vertical partial derivatives):

$$\rho_t + \underline{u}^h.\nabla\rho + w.\rho_z = K_v\rho_{zz} + K_h\nabla^2\rho + S, \qquad (1)$$

where ρ, $\underline{u}^h$, w, K_v, K_h and S denote respectively the density field, the horizontal and vertical velocity fields, the vertical and horizontal diffusion coefficients, and the surface density fluxes. Since the annually-averaged stratification is stable, and since the vertical coordinate z increases upward, ρ_z is negative everywhere.

In the following sections, we shall focus on the mean state of the ocean interior, which is not directly affected by atmospheric fluxes S, nor by convective events. The first and last terms in equation (1) will thus be neglected and our investigations restricted to south of about 50°N. Away from convection regions, after a temporal averaging, equation (1) provides the following expression for the annual mean vertical velocity field w:

$$w = \overbrace{-\frac{1}{\rho_z}\underline{u}^h.\nabla\rho}^{w_i} + \overbrace{\underbrace{\frac{1}{\rho_z}K_v\rho_{zz}}_{w_{cV}} + \underbrace{\frac{1}{\rho_z}K_h\nabla^2\rho}_{w_{cH}}.}^{w_c} \qquad (2)$$

In this equation, w is expressed as the sum of its isopycnal (w_i) and diapycnal (w_c) components. Diapycnal velocities w_c can be induced by vertical and horizontal diffusion, the respective contributions of which are denoted by w_{cV} and w_{cH}. The terms w, w_i, w_{cV} and w_{cH} were diagnosed from the annual mean density and velocity fields, interpolated and smoothed along the five selected isopycnal surfaces, and averaged between 24°W and 16°W. Along such a steady isopycnal surface, a positive value of w_{cV} (respectively, w_{cH}) means that vertical (respectively, horizontal) diffusion induces an upward transport across the surface which tends to inflate the lighter layer located above the isopycnal at the expense of the heavier one located below, and therefore to decrease the density averaged over this pair of layers. Since the annually averaged density field is steady, such a trend in the density equation (2) must be compensated for by other terms.

Despite the fact that the values of K_v and K_h are set by numerical stability requirements and may be overestimated in the model, and that some processes known to induce diapycnal mass transfers (like double-diffusion below the MW intrusion [*Arhan,* 1987; *Paillet et al.,* 1998]) are not taken into account, our annually-averaged numerical solution may provide information about the origin and the effect of w_{cV} and w_{cH} on the meridional circulation in the intergyre zone.

Equation (2) cannot be verified exactly in the steady state solution, because density is a diagnostic quantity of the model and because surface fluxes force convective mixing down to a certain level. In addition, we have used simple averaging and interpolating procedures. A verification of the buoyancy balance (2) is thus necessary before interpreting our results, even in terms of trends. The maximum residual vertical velocity tolerated in equation (2) was arbitrarily set to $w_{\rm lim} = 2 \times 10^{-7}$ m s^{-1}. The aim of Figure 8 is to highlight the regions where our results may make sense, i.e. where the residual in equation (2) (the difference between w_c and $w - w_i$) is smaller than $w_{\rm lim}$. In this and subsequent figures, thick lines indicate where this criterion is verified. Equation (2) appears to be more correct along the three upper isopycnal surfaces than along the other two (the model dynamics in isopycnal layers 3 and 4 will thus be interpreted with caution), but some large-scale trends make sense everywhere. Figure 9 presents the meridional profiles of w_{cV} and w_{cH} along the five selected isopycnal surfaces.

4.1.2. The vorticity balance. In the isopycnal layers of Table 4, we shall investigate how the model mean meridional circulation, averaged between 24°W and 16°W, is influenced by the different components of vertical stretching. Let us consider an isopycnal layer of local thickness Δz, and let V_p denote the layer-averaged local meridional circulation induced by

Δw, the vertical velocity difference between the upper and lower limits of the layer. The large-scale vorticity balance gives

$$V_p = \frac{f}{\beta}\frac{\Delta w}{\Delta z}, \quad (3)$$

where f and β denote the Coriolis parameter and its meridional gradient respectively. Figure 10 shows that the large-scale trends of V are globally controlled by vertical stretching ($V \sim V_p$), in particular within the two uppermost isopycnal layers. Substituting (2) in (3) gives the following expression for V_p:

$$V_p = V_{pi} + V_{pV} + V_{pH}, \quad (4)$$

where V_{pi}, V_{pV} and V_{pH} (shown in Figure 11) denote the meridional velocities driven by the vertical stretching of w_i, w_{cV}, and w_{cH}, respectively.

4.2. The dynamical impact of diffusion

The contributions of vertical and horizontal diffusion to the buoyancy balance (w_{cV} and w_{cH}, respectively) are shown in Figure 9 for each of the five selected isopycnal surfaces. The meridional circulations V_{pV} and V_{pH} driven by these respective diapycnal transfers in the four isopycnal layers through vortex stretching are shown in Figure 11.

4.2.1. Vertical diffusion.

4.2.1.1. Layer 1: Along the isopycnal surface 26.9, located below the surface stratification south of 40°N, ρ_{zz} is negative. Since ρ_z is also negative, vertical diffusion induces an upward diapycnal velocity w_{cV} (Figure 9). Since w_{cV} is weaker along the isopycnal surface 27.1, vertical diffusion induces stretching in layer 1 and therefore a northward motion within the upper SPMW (Figure 11). The strong w_{cV} maximum visible in Figure 9 between 40°N and 48°N along the uppermost isopycnal surface is due to the vertical penetration through vertical diffusion of the atmospheric buoyancy input (S is important here). Since the residual in equation (2) largely exceeds $w_{\rm lim}$, we will not interpret this feature further.

4.2.1.2. Layer 2: The isopycnal surface 27.1 lies near the potential vorticity minimum associated with the subducted SPMW south of 40°N, but is located underneath it north of 40°N (Figure 7). The diapycnal velocity w_{cV}, which is negatively correlated with ρ_{zz}, is thus weak south of 40°N and negative further north (Figure 9). South of 40°N, w_{cV} does not differ much along the upper and lower limits of layer 2 (isopycnal surfaces 27.1 and 27.4 in Figure 9). Vertical diffusion thus induces no significant meridional motion V_{pV} within the dense SPMW (Figure 11). North of 40°N in layer 2, vertical diffusion shrinks layer 2 and drives a southward motion.

4.2.1.3. Layers 3 and 4: Below the main thermocline along the isopycnal surfaces 27.4, 27.6, and 27.8, ρ_z and ρ_{zz} are negative. Vertical diffusion thus induces a positive diapycnal velocity w_{cV} across these surfaces (Figure 9), in accordance with the classical theory of *Stommel and Arons* [1960]. Since ρ_z tends to zero downwards, w_{cV} increases downwards: through vortex stretching, vertical diffusion induces an equatorward flow within the tongue of MW (V_{pV} in Figure 11, layer 3). Despite the noisy character of our computations in layer 4, Figure 11 suggests that the same process drives a southward motion of LSW.

To summarize, vertical diffusion induces a rather simple baroclinic meridional circulation V_{pV} through vortex stretching in the intergyre zone (except north of 40°N in the upper and lower SPMW where the situation is more complex): A poleward flow opposite to the mean advection (see V in Figure 10) within layer 1 that vanishes in layer 2; an equatorward flow in layer 3, like V, suggesting that the southward advection within the MW tongue is promoted by vertical diffusion. The equatorward motion of LSW simulated by the model north of about 35°N is also promoted by vertical diffusion.

4.2.2. Horizontal diffusion. The diapycnal velocity field induced by horizontal diffusion (w_{cH} in Figure 9) exhibits a more complex structure. We first describe its large-scale characteristics, and then briefly present its content at smaller scales.

4.2.2.1. Large-scale tendencies: Along the isopycnal surfaces 27.1 and 27.4 which constitute the upper and lower limits of layer 2 (dense SPMW), w_{cH} exhibits opposite large-scale meridional tendancies (northward increase along 27.1 and decrease along 27.4), related to the curvature of isopycnal surfaces. Between 33°N and 42°N within the lower SPMW, the subsequent vertical stretching thus induces a northward motion (V_{pH} in Figure 11) which counteracts the equatorward motion of dense SPMW simulated by the model (V in Figure 10). Along the isopycnal surfaces 27.4 and 27.6, w_{cH} decreases northward in a similar fashion indicating that horizontal diffusion does not drive any large-scale meridional circulation through vortex stretching in the MW tongue (Figure 11). However, w_{cH} remains globally constant along the isopycnal surface 27.8. In layer 4 (LSW), horizontal diffusion contributes to the simulated equatorward flow V north of about 40°N and opposes it

south of 40°N.

4.2.2.2. Smaller scales: The diapycnal velocity w_{cH} induced by horizontal diffusion also varies at scales of about 600 km. Figure 9 shows a regular succession of w_{cH} extrema near 35°N, 40°N, and 45°N-48°N throughout the water column. The southernmost peak is visible along the northern flank of the AC (35°N) where the four uppermost isopycnal surfaces exhibit a dome-like shape (Figure 7). Horizontal diffusion tends to flatten this curvature an lighten the water column. Through vertical stretching, this diffusive effect locally intensifies the equatorward flow V in layer 1, and counteracts it in layers 3 and 4 (Figure 11).

The w_{cH} local minimum (density gain) diagnosed at 40°N across the four uppermost isopycnal surfaces (and at 47°N across 27.4 and 27.6) comes from the local tendency of the isopycnal surfaces to rise northward. Since these minima are not located at exactly the same latitude, their effect on meridional motions is complex and difficult to interpret.

4.3. Adiabatic and Diabatic Motions - Summary

The impact of diffusion on the intergyre circulation is now compared with the adiabatic motion V_{pi} that could exist within the isopycnal layers without any diapycnal mass flux, between solid isopycnal surfaces. Unlike V_{pV} and V_{pH}, which are forced locally by diapycnal eddy fluxes, V_{pi} is forced in the regions where the density layers outcrop (by high latitude convection or Ekman pumping). A motion may thus be considered as adiabatic where V_{pV} and V_{pH} are smaller than V_{pi}.

Comparing Figure 10 and Figure 11 shows that the meridional stuctures of V and V_{pi} are similar south of 46°N in layers 1 and 2. Within the SPMW, the model behavior is comparable to the idealized ventilated thermocline solutions, but the ventilation of SPMW is slowed by eddy diffusion effects (vertical diffusion in the upper SPMW, horizontal diffusion in the lower SPMW). The situation is comparable north of about 45°N in layer 3, where the realistic poleward flow of MW simulated by the model could exist without diapycnal mixing (V and $V_{pi} > 0$). This corroborates the analytical results of *Schopp and Arhan* [1986] based on the ventilated thermocline adiabatic hypothesis. The northern part of the MW is probably driven northward by positive Ekman pumping in the subpolar gyre, where our third layer outcrops. As for the SPMW, the model suggests that this motion is slowed down by horizontal diffusion, perhaps too much since V is rather weak. We mentioned above that the observed poleward motion of MW is not simulated by the model between 36°N and 45°N. From a local analysis based on in situ data, *Arhan* [1987] demonstrated that this motion may be driven by salt fingering below the MW intrusion. This mechanism, which generates up-gradient density fluxes through differential salinity and temperature vertical diffusion, is not parameterized in the model. If this process is actually at work and significant throughout the basin, the subsequent northward motion is thus not expected to be simulated by the model south of 45°N.

The downward decrease of ρ_z below the main thermocline is likely to induce a downward increase of w_{cV}, a negative V_{pV} through vortex stretching, and a southward motion of diabatic origin within layers 3 and 4. Indeed, within the MW and LSW V_{pi} does not follow V as well as within the SPMW. South of 45°N in fact, vertical diffusion tends to promote or even force the simulated southward flow of MW and LSW, especially around 40°N where no adiabatic meridional motion is possible ($V_{pi} \sim 0$), and in the MW around 37°N where V_{pi} is totally compensated for by V_{pH}.

Our interpretation of the MW and LSW motions may be compared to that of *Spall* [1999], who used a steady $2\frac{1}{2}$-layered planetary geostrophic model similar to that of *Luyten and Stommel* [1986], but where meddies, turbulent isopycnal mixing, and diapycnal fluxes forced by salt fingering are parameterized. Spall obtains realistic circulation patterns for both water masses in the eastern basin (roughly northward for upper MW and southward for lower MW and LSW) mostly driven by salt fingering, as diagnosed locally by *Arhan* [1987] within the upper MW. This suggests that the southward motion of LSW may be forced either by the stretching induced by vertical diffusion (absent from Spall's model) or by double-diffusion (not parameterized in our model). The inability of our model to reproduce the northward motion of MW between 36°N and 45°N may be linked to the absence of double-diffusion, but confirmation of this hypothesis will require further investigation.

5. Conclusion

The aims of this work were to describe and validate the mean solution obtained in a coarse-resolution regional model of the eastern North Atlantic, and to investigate the large-scale equilibrium dynamics of the intergyre zone. The computational domain is re-

stricted to the basin of interest through the use of three self-adapting open boundaries that leave the barotropic currents locally unconstrained. The model is integrated over 38 years with a variable surface and baroclinic lateral forcing, and reaches a steady annual-mean state (modulated by the seasonal cycle) despite the wide opening of the basin to the rest of the Atlantic. The final annually-averaged circulation, stratification and forcing are adjusted mutually and provide a plausible picture of the ocean mean state in the basin.

The North Atlantic Current (NAC) brings about 40 Sv into the eastern basin above the Mid-Atlantic Ridge (MAR), where it shifts slightly northward. As shown in recent studies, 30% of this transport can be attributed to the vertical velocities induced by bottom currents along sloping topography. East of the MAR, the NAC splits into 3 main branches whose paths and transports agree with different in situ estimates. Two thirds of the NAC recirculates toward the subpolar gyre. A 13-Sv Irminger Current circulates cyclonically and joins the East Greenland Current which transport reaches the realistic value of 40 Sv.

South of about 47°N above 800 m, 4.5 Sv of thermocline waters are advected toward a realistic Azores Current (AC), which transport exceeds 9 Sv across 35°W and decreases eastward. As far as we know, the AC had never been simulated by coarse-resolution models. The combined use of a self-adapting western open boundary, which only constrains the baroclinic structure of currents that enter the domain, and of a T-S climatology [*Reynaud et al.,* 1998] that represents the density fronts quite well partly explains this interesting feature. Unlike in Levitus' widely-used climatologies, the Azores Front is present in our initial density field and geostrophically generates the AC within a few inertial periods. Like the NAC, the baroclinic structure of the incoming AC is then maintained for the whole integration at 40°W. Unlike another wind data set that we used in a sensitivity experiment [*Penduff,* 1998], the wind climatology of *Hellermann and Rosenstein* [1983] also contribute to the presence of the AC since its mean curl forces an eastward flow between 30°N and 35°N (Figure 5). The local entrainment of surface waters into the MW in the Gulf of Cadiz, parameterized by a simple relaxation of tracers, also tends to increase the AC transport.

South of the NAC above 2000 m, most observed circulation patterns are fairly well simulated. Their dynamical origin was investigated through the buoyancy and vorticity balances. The southward motion of thermocline waters and Subpolar Mode Water agrees with previous studies and is consistent with a ventilated thermocline adiabatic solution, globally slowed down by diffusive effects. A similar dynamical regime is found between 500 and 1000 m north of 45°N, where the MW realistically flows northward. Positive Ekman pumping in the subpolar gyre is likely to drive the northward motion of MW adiabatically, as shown by *Schopp and Arhan* [1986] with a model of the ventilated thermocline; this flow is slowed down in the present model by eddy diffusive effects. South of 45°N, vertical diffusion induces a slow southward drift of the MW through vortex stretching, instead of the observed northward flow. The absence in the model of any parametrization of salt fingering beneath the MW intrusion, a process which could force the observed motion [*Arhan,* 1987; *Spall,* 1999], is a possible explanation for this discrepancy. Another explanation is the crude representation of the MW overflow process in the Gulf of Cadiz and of the subsequent spreading of the MW into the Atlantic (simple relaxation of tracers and closed boundary near the Strait of Gibraltar, coarse resolution, smoothed topography).

The paths and transports of Labrador Sea Water (LSW) over the entire basin agree well with observations. As in the case of the MW, our analysis suggests that its southward motion is mainly driven by the vertical stretching induced by vertical diffusion. However, a realistic LSW large-scale flow similar to ours was obtained by *Spall* [1999], under the influence of salt fingering through the lower interface of MW, without vertical diffusion. Therefore, both effects may contribute to the southward motion of LSW across the basin.

Our computation of the terms involved in the buoyancy and vorticity balances is rather simple and could be improved. First, our annually-averaged solution represents a steady climatological state that is largely modulated by interannual variability in the real ocean, especially within the intergyre zone as noted in the introduction; the use of an interannual surface forcing would certainly generate a more realistic fluctuating regime in the intergyre zone. On the other hand, the explicit representation of mesoscale eddies, a better vertical resolution, and an efficient parametrization of salt fingering are likely to make the model solution and of our diagnostics more realistic. In the future, an on-line computation of diffusive terms would be necessary to close the buoyancy and vorticity balances, and to quantify the contribution

of the mesoscale eddies.

Acknowledgments. This research was supported by a DRET doctoral fellowship for 3 years, and by a SHOM research contract for the 4th year.

References

Arhan, M., On the large scale dynamics of the Mediterranean outflow, *Deep Sea Res.*, *34*, 1187-1208, 1987.

Arhan, M., A. Colin de Verdiere, and H. Mercier, Direct observations of the mean circulation at 48°N in the Atlantic Ocean, *J. Phys. Oceanogr.*, *19*, 161-181, 1989.

Bacon, S., Decadal variability in the outflow from the Nordic Seas to the deep Atlantic Ocean, *Nature*, 394, 27 August 1998.

Barnier, B., L. Siefridt, and P. Marchesiello, Thermal forcing for a global ocean circulation model using a three-year climatology of ECMWF analyses, *J. Mar. Syst.*, *6*, 363-380, 1995.

Barnier, B., P. Marchesiello, A.P. de Miranda, J.M. Molines, and M. Coulibaly, A sigma-coordinate primitive equation model for studying the circulation in the South Atlantic, I, Model configuration with error estimates, *Deep Sea Res.*, *45*, 573-608, 1998.

Brügge, B., Near-surface mean ciculation and kinetic energy in the central North Atlantic from drifter data, *J. Geophys. Res.*, *100*, 20,543-20,554, 1995.

Dickson, R.R., J. Gould, T.J. Müller, and C. Maillard, Estimates of the mean circulation in the deep (> 2000m) layer of the eastern North Atlantic, *Prog. Oceanog.*, *14*, 103-127, 1985.

Dickson, R.R., and J. Brown, The production of North Atlantic Deep Water: Sources, rates, and pathways, *J. Geophys. Res.*, *99*, 12,319-12,341, 1994.

DYNAMO Group, *DYNAMO, Dynamics of North Atlantic Models: Simulation and Assimilation with High Resolution Models*, 334 pp., Inst. für Meereskunde, Kiel, Germany, 1997.

Gana, S., and C. Provost, Circulation and fluxes of the Central Atlantic in 1983/1984 estimated by inverse analysis of "Topogulf" hydrographic data, *J. Mar. Syst.*, *4*, 67-92, 1993.

Hellermann, S., and M. Rosenstein, Normal monthly wind stress on the world ocean with error estimates, *J. Phys. Oceanogr.*, *13*, 1093-1104, 1983.

Kelly, K., The meandering Gulf Stream as seen by the Geosat altimeter: Surface transport, position and velocity variance from 73°W to 46°W, *J. Geophys. Res.*, *96*, 16,721-16,738, 1991.

Klein, B., and G. Siedler, On the Origin of the Azores Current, *J. Geophys. Res.*, 94, 6159-6168, 1989.

Knochel, H., Développement et validation d'un modèle numérique de circulation océanique à coordonnées σ pour l'étude climatique de l'Atlantique Nord, thèse, Univ. J. Fourier, 210 pp., Grenoble, France, Dec. 1998.

Krauss, W., E. Fahrbach, A. Aitsam, J. Elken, and P. Koske, The North Atlantic Current and its associated eddy field southeast of Flemish Cap, *Deep Sea Res.*, *34*, 1163-1185, 1987.

Luyten, J.R., J. Pedlosky, and H. Stommel, The ventilated thermocline, *J. Phys. Oceanogr.*, *13*, 292-309, 1983.

Luyten, J.R., and H. Stommel, Gyres driven by combined wind and buoyancy flux, *J. Phys. Oceanogr.*, *16*, 1551-1560, 1986.

Maillard, C., Atlas hydrologique de l'Atlantique Nord-Est, 32 pp, Institut Français de Recherche pour l'Exploitation de la Mer, Brest, France.

McCartney, M.S., and L.D. Talley, Warm-to-Cold Water Conversion in the Northern North Atlantic Ocean, *J. Phys. Oceanogr.*, *14*, 922-935, 1984.

Orvik, K.A., O. Skagseth, and M. Mork, Atlantic inflow to the Nordic Seas in the Svinoy section, *Int. WOCE Newsl.*, *37*, 18-20, 1999.

Otto, L., and H.M. van Aken, Surface Circulation in the northeast Atlantic as observed with drifters, *Deep Sea Res.*, *43*, 467-499, 1996.

Paillet, J., and M. Arhan, Shallow pycnoclines and mode water subduction in the eastern North Atlantic, *J. Phys. Oceanogr.*, *26*, 96-114, 1996.

Paillet, J., M. Arhan, and M.S. McCartney, Spreading of Labrador Sea Water in the eastern North Atlantic, *J. Geophys. Res.*, *103*, 10223-10239, 1998.

Paillet, J., and H. Mercier, An inverse model of the eastern North Atlantic general circulation and thermocline ventilation, *Deep Sea Res.* I, *44*, 1293-1328, 1997.

Penduff, T., Etude de la dynamique de l'Atlantique Nord-Est à l'aide d'un modèle numérique régional, thèse, Univ. de Bretagne Occidentale, 261 pp., Brest, France, Oct. 1998.

Penduff, T., A. Colin de Verdière, and B. Barnier, Self-adapting open boundaries for a sigma coordinate model of the eastern North Atlantic, *J. Geophys. Res.*, in press.

Reid, J.L., On the total geostrophic circulation of the North Atlantic Ocean: Flow patterns, tracers and transports, *Prog. Oceanog.*, *33*, 1-92, 1994.

Reynaud, T., P. Legrand, H. Mercier, and B. Barnier, A new analysis of hydrographic data in the Atlantic and its application to an inverse modelling study, *WOCE Newslett.*, *32*, 29-31, Sept. 1998.

Saunders, P.M., Circulation in the eastern North Atlantic, *J. Mar. Res.*, *40*, Supplement, 641-657, 1982.

Saunders, P.M., The flux of Overflow Water through the Charlie-Gibbs Fracture Zone, *J. Geophys. Res.*, *99*, 12,343-12,355, 1994.

Schmitz, W.J. Jr, and M.S. McCartney, On the North Atlantic circulation, *Rev. of Geophys.*, *31*, 1, 29-49, 1993.

Schopp, R., and M. Arhan, A ventilated middepth circulation model for the eastern North Atlantic, *J. Phys. Oceanogr.*, *16*, 344-357, 1986.

Schott, F.A., and C. Böning, Evaluation of the WOCE model in the western equatorial Atlantic: Upper layer circulation, *J. Geophys. Res.*, *96*, 6993-7004, 1991.

Siedler, G., and R. Onken, Eastern recirculation, in *The Warmwatersphere of the North Atlantic Ocean*, edited by W. Krauss, pp. 339-364, Gebrüder Borntraeger, Berlin, 1996.

Spall, M.A., A simple model of the large-scale circulation of Mediterranean Water and Labrador Sea Water, *Deep Sea Res.*, *46*, 181-204, 1999.

Speer, K.G., J. Gould, and J. LaCasce, Year-long trajectories in the Labrador Sea Water of the eastern North Atlantic Ocean, *Deep Sea Res.*, *46*, 165-179, 1999.

Stommel, H., and A.B. Arons, On the abyssal circulation of the world ocean, II, an idealized model of the circulation pattern and amplitude in oceanic basins. *Deep Sea Res.*, *6*, 217-233, 1960.

Stramma, L., Geostrophic transport in the warm water sphere of the eastern subtropical North Atlantic, *J. Mar. Res.*, *42*, 537-558, 1984.

Sy, A., Investigation of large-scale circulation patterns in the central North Atlantic: The North Atlantic Current, the Azores Current, and the Mediterranean Water plume in the area of the Mid-Atlantic Ridge, *Deep Sea Res.*, *35*, 383-413, 1988.

Sy, A., V. Schauer, and J. Meincke, The North Atlantic Current and its associated hydrographic structure above and eastwards of the Mid-Atlantic Ridge, *Deep Sea Res.*, *39*, 825-853, 1992.

Treguier, A.M., Kinetic energy analysis of an eddy-resolving, primitive equation model of the North Atlantic, *J. Geophys. Res.*, *97*, 687-701, 1992.

Wegner, G., Geostrophische Oberflächenströmung im nördlichen Nordatlantischen Ozean im internationalen geophysikalischen Jahr 1957/58, *Ber. Dtsch. Wiss. Komm. für Meeresforsch.*, *22*, 411-426, 1973.

Wunsch, C., and D. Roemmich, Is the North Atlantic in Sverdrup Balance? *J. Phys. Oceanogr.*, *15*, 1876-1880, 1985.

B. Barnier and T. Penduff, Laboratoire des Écoulements Géophysiques et Industriels, UMR 5519 CNRS, BP 53X,
38041 Grenoble Cedex, France. (Bernard.Barnier@hmg.inpg.fr; Thierry.Penduff@hmg.inpg.fr)

A. Colin de Verdière, Laboratoire de Physique des Océans, UMR 6523, Université-CNRS-IFREMER, Université de Bretagne Occidentale, Brest, France. (Alain.Colin-De-Verdiere@univ-brest.fr)

January 3, 2000; revised February 27, 2000; accepted March 31, 2000.

Figure 1. The eastern North Atlantic original topography. Straight lines represent the computational domain limits.

Figure 2. Model topography in m. Plain lines locate the northern fixed boundaries where the model variables are prescribed; dashed lines locate the three self-adaptative open boundaries; unshaded three-gridpoint square regions at the southwestern and northeastern corners correspond to artificial islands (necessary at the intersection of two open boundaries).

Figure 3. Scheme of the model circulation showing the horizontal transports (Sv) in three different layers: (a) 0 - 800 m including the Ekman transport; (b) 800 - 1500 m; and (c) 1500 m - bottom. Vertical transports between the layers are underlined (in Sv), and close the local volume budgets; arrows are drawn where the vertical transports are maximum. Horizontal and vertical straight lines are drawn every ten degrees of longitude and latitude starting from (40°W, 30°N) in the southwestern corner.

Figure 4. Mean barotropic stream function ψ (Sv). In this and subsequent Figures of ψ, unshaded regions correspond to cyclonic circulations, shaded regions correspond to anticyclonic circulations; the contour interval is 2 Sv.

Figure 5. Sverdrup barotropic stream function (Sv), given by the westward integration of the wind stress curl from *Hellermann and Rosenstein* [1983]'s annual climatology. Contour interval is 2 Sv.

Figure 6. (top) Model meridional velocity (in 10^{-2} m s^{-1}) at four latitudes in the model, averaged over the last year of integration and between 24°W and 16°W. (bottom) Mean geostrophic velocity (in 10^{-2} m s^{-1}) east of the Mid-Atlantic Ridge at the same latitudes, computed by *Saunders* [1982] from in situ data with a reference level at 4000 m. Note the change of vertical scale at 1000 m.

Figure 7. Mean large-scale potential vorticity (PV $= -f\rho_z$) and density fields averaged between 24°W and 16°W. The thick blue line locates the PV minimum associated with the core of SPWM, the thick black line locates the PV maximum associated with the main thermocline.

Figure 8. The balance between w_c and $w - w_i$ (10^{-7} m s^{-1}) along the isopycnal surfaces 26.9, 27.1, 27.4, 27.6 and 27.8. Thick segments indicate the regions where the two terms differ by less than 2.10^{-7} m s^{-1}, and where equation (2) will thus be considered as correctly valid. Both quantities have been averaged in the band 24°W - 16°W.

Figure 9. The two components of w_c (in 10^{-7} m s^{-1}), averaged between 24°W and 16°W, along the isopycnal surfaces 26.9, 27.1, 27.4, 27.6 and 27.8. Thick lines as in Figure 8.

Figure 10. Meridional velocity V_p driven by vertical stretching Δw, and model mean meridional velocity V (in 10^{-2} m s^{-1}). Both terms are averaged between 24°W and 16°W and within the four isopycnal layers of Table 4. Lines are thickened where equation (2) has been validated along the upper and along the lower interfaces of each layer.

Figure 11. The three components of V_p (in 10^{-2} m s^{-1}) averaged annually, between 24°W and 16°W, and within the four isopycnal layers of Table 4. Thick lines as in Figure 10.

Table 1. Net Transports Prescribed Across The Domain Boundaries

Boundary	Net Transports, Sv
Western OB[a]	15 Sv eastward
Southern OB[a]	15 Sv southward
Eastern OB[a]	11 Sv eastward
Northwestern FB[b]	9 Sv southward
Northeastern FB[b]	2 Sv southward

[a]OB denotes a self-adapting open boundary. Along the OBs, the profile of the barotropic stream function ψ is entirely diagnostic, without any relaxation.

[b]FB denotes a fixed boundary. Along the FBs, the ψ profile is set equal to a fixed linear profile.

Table 2. Timescales τ Used Along the Western, Eastern, and Southern Self-Adapting Open Boundaries (OBs) for the Relaxation of the Model Baroclinic Variables to Climatology

Model Variable	τ in Outflow regime	τ in Inflow regime
Temperature, Salinity	5 years	15 days
Baroclinic normal velocity	5 years	3 days
Total tangential velocity	5 years	3 days

Climatological values for the tracers come from the seasonal climatology of *Reynaud et al.* [1998] (noted RLM); climatological values for the baroclinic normal velocity field geostrophically derive from the RLM density fields (their depth-averaged component is removed at each point of the boundary); the climatological value for the total tangential velocity field is zero.
In addition to this relaxation, outgoing barotropic and baroclinic perturbations are radiated away through the OBs. The barotropic stream function ψ is never relaxed to any climatological profile along the OBs, that is $\tau_\psi = \infty$ at each time step and each grid point in outflow and in inflow regimes.

Table 3. Model Parameters and Surface Forcing

Model Parameter	Value
	Spatial and temporal resolution
Horizontal resolution Δ	Isotropic, $\Delta = 0.8°$ in longitude, $0.8° \times cos(\phi)$ in latitude ϕ: Δ=77 km at 30°N, Δ=35 km at 66.5°N.
Vertical resolution Δ_Z	Twenty-one sigma levels, Δ_Z ranges from 11 m to 28 m near the surface, from 48 m to 671 m near the bottom
Time step	One hour
	Parametrization of subgrid scale processes
Bottom friction	Linear law; the coefficient is 2.65×10^{-4} s^{-1}
Horizontal turbulent viscosity	$3000 \times \Delta/\Delta_{max}$ m^2 s^{-1}($laplacianoperator$)
Horizontal turbulent diffusivity	$875 \times \Delta/\Delta_{max}$ m^2 s^{-1}($laplacianoperator$)
Vertical turbulent viscosity	10^{-4} m^2 s^{-1} (10^{-3} in the top 50 m)
Vertical turbulent diffusivity	10^{-4} m^2 s^{-1} (10^{-3} in the top 50 m)
In case of static instability:	The vertical diffusivity is set to 1 m^2 s^{-1}, and a convective adjustment is made every day where necessary
	Surface forcing[a]*, applied as a body force on the top 50 m*
Heat flux	Monthly ECMWF[b] heat flux with a relaxation of the sea surface temperature to seasonal RLM[c] values
Salt flux	Relaxation of the sea surface salinity to seasonal RLM[c] values
Wind stress	*Hellermann & Rosenstein* [1983] monthly climatology
	Parametrization of the Mediterranean Water overflow
Relaxation timescale of tracers	30 days in the Gulf of Cadiz at all depths to RLM[c] seasonal values; Gibraltar Straits is closed

[a]This surface forcing is adapted from *Barnier et al.* [1995].

[b]ECMWF refers to the European Centre for Medium-Range Weather Forecasts.

[c]RLM refers to *Reynaud et al.* [1998]'s T-S seasonal climatology.

Table 4. Density Range and Water Mass Embedded Within Each of the Four Isopycnal Layers Considered in Section 4

Layer number	Density range	Water mass
1	$26.9 < \sigma_0 < 27.1$	Upper Subpolar Mode Water
2	$27.1 < \sigma_0 < 27.4$	Lower Subpolar Mode Water
3	$27.4 < \sigma_0 < 27.6$	Mediterranean Water
4	$27.6 < \sigma_0 < 27.8$	Labrador Sea Water

Table 4. (continued)

Layer number	Density range	Water mass

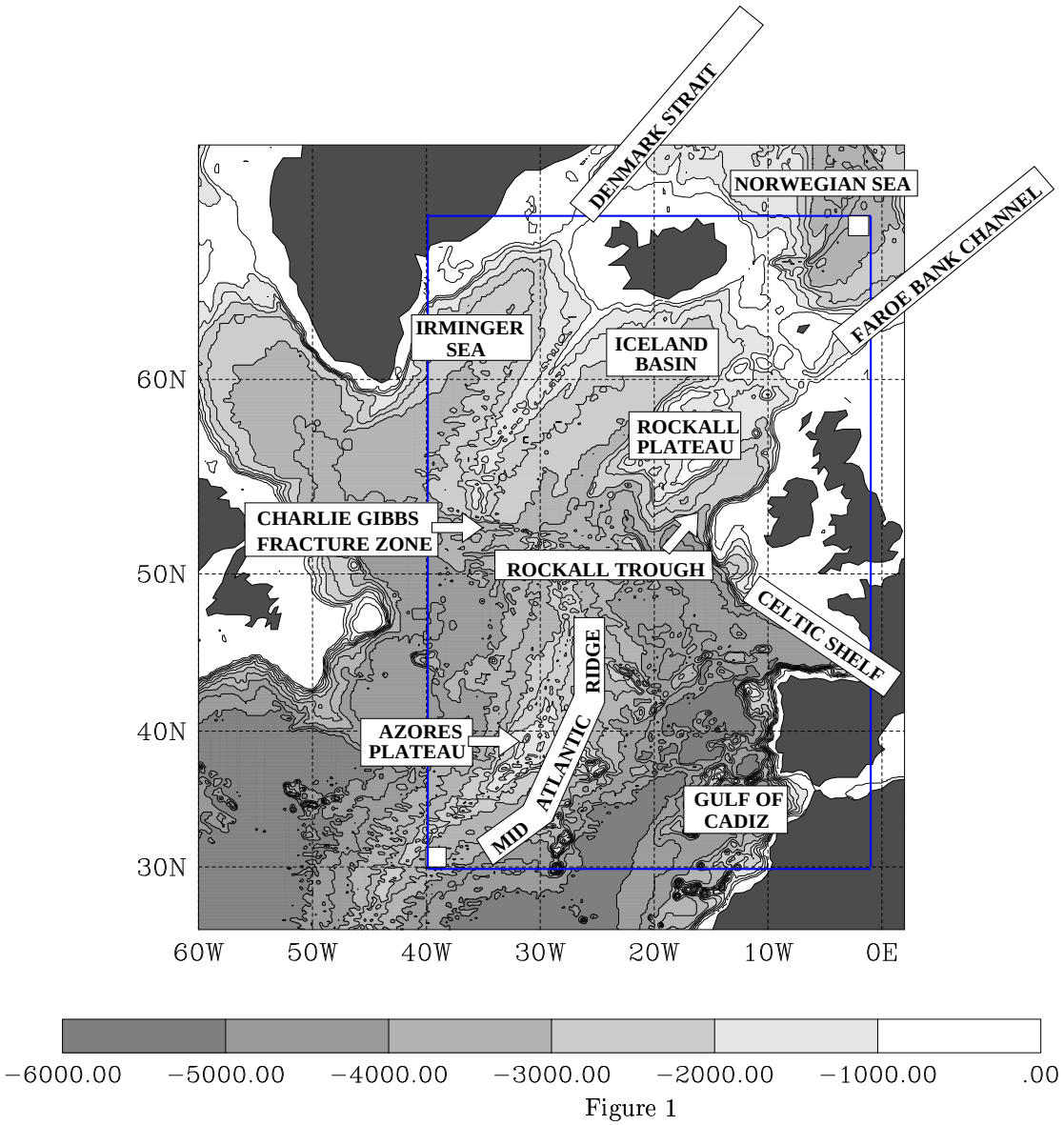
DENMARK STRAIT
NORWEGIAN SEA
FAROE BANK CHANNEL
IRMINGER SEA
ICELAND BASIN
ROCKALL PLATEAU
CHARLIE GIBBS FRACTURE ZONE
ROCKALL TROUGH
CELTIC SHELF
MID ATLANTIC RIDGE
AZORES PLATEAU
GULF OF CADIZ
60N
50N
40N
30N
60W
50W
40W
30W
20W
10W
0E
−6000.00
−5000.00
−4000.00
−3000.00
−2000.00
−1000.00
.00

Figure 1

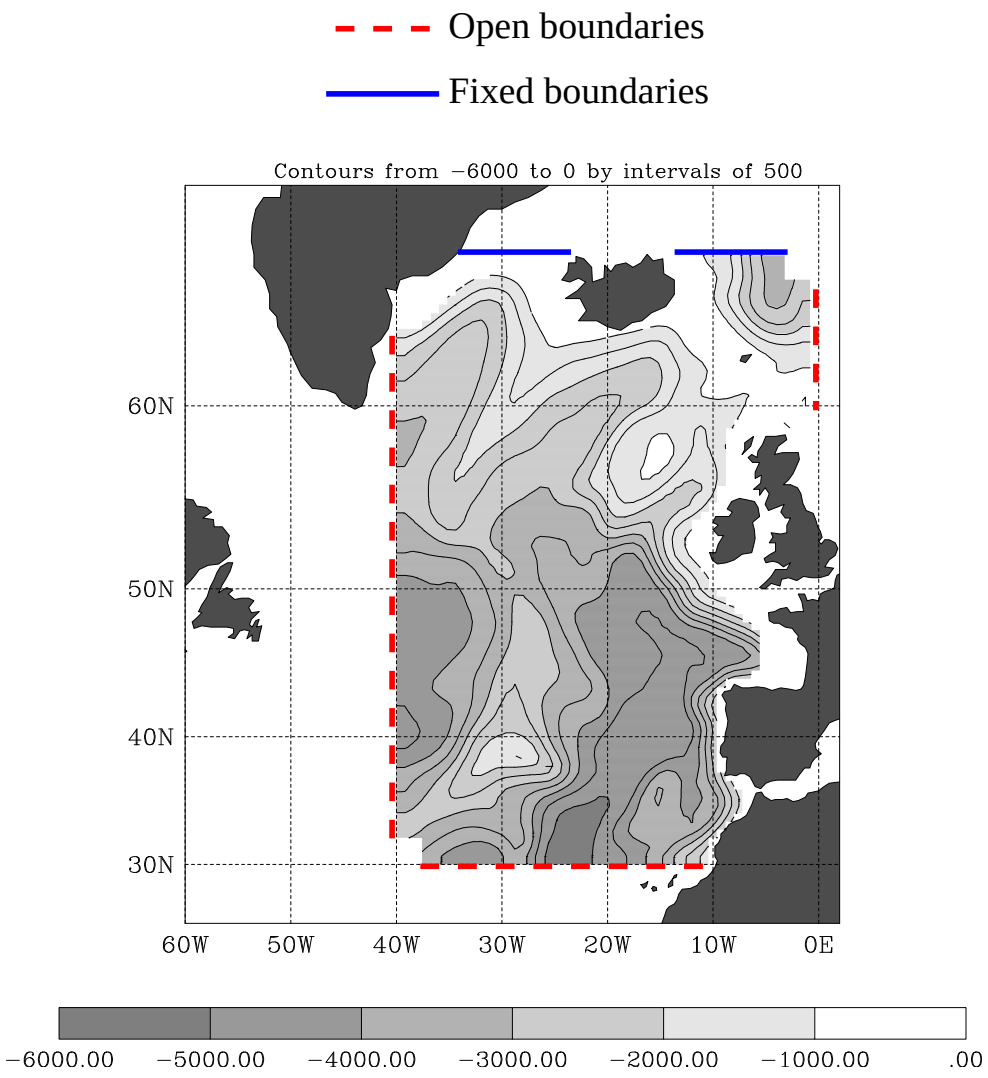
Open boundaries
Fixed boundaries
Contours from −6000 to 0 by intervals of 500
60N
50N
40N
30N
60W
50W
40W
30W
20W
10W
0E
−6000.00
−5000.00
−4000.00
−3000.00
−2000.00
−1000.00
.00

Figure 2

.

Figure 3

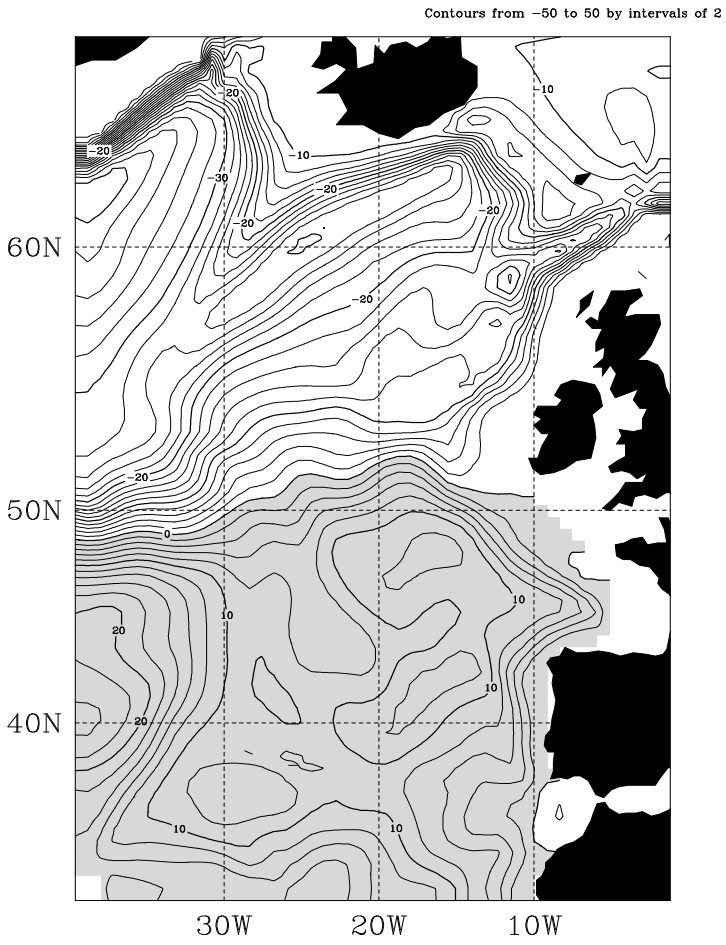
BAROTROPIC STREAMFUNCTION – YEAR 38
Contours from −50 to 50 by intervals of 2
60N
50N
40N
30W
20W
10W

Figure 4

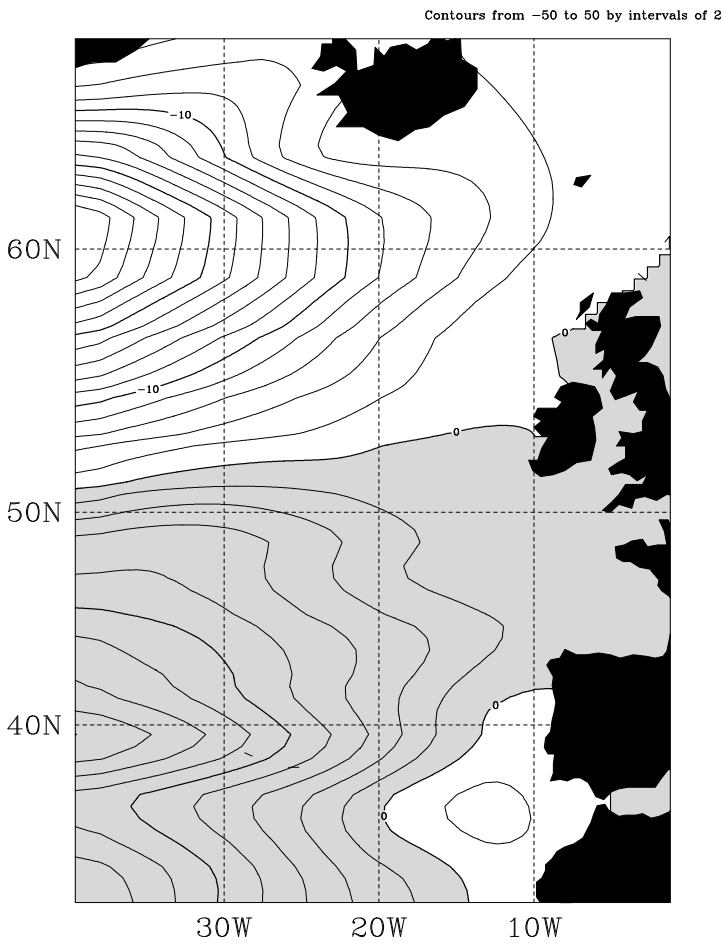
MEAN SVERDRUP STREAMFUNCTION
Contours from −50 to 50 by intervals of 2
−10
−10
0
0
0
0
60N
50N
40N
30W
20W
10W

Figure 5

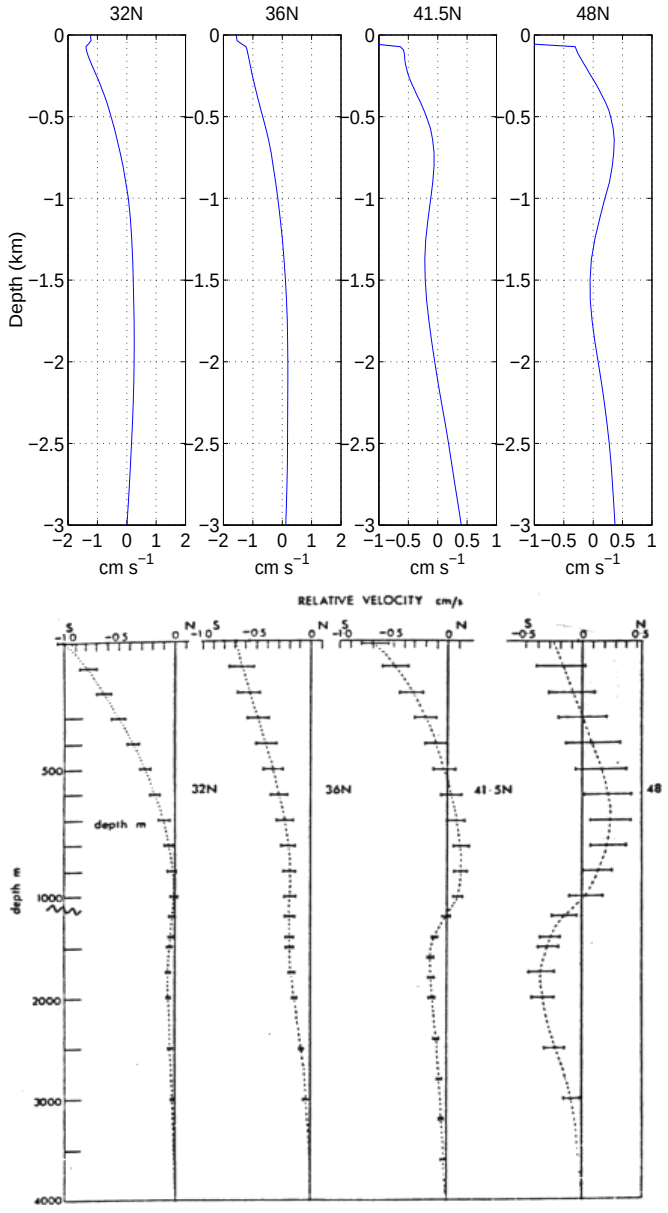
32N
36N
41.5N
48N
Depth (km)
cm s^{-1}
RELATIVE VELOCITY cm/s
depth m
32N
36N
41·5N
48

Figure 6

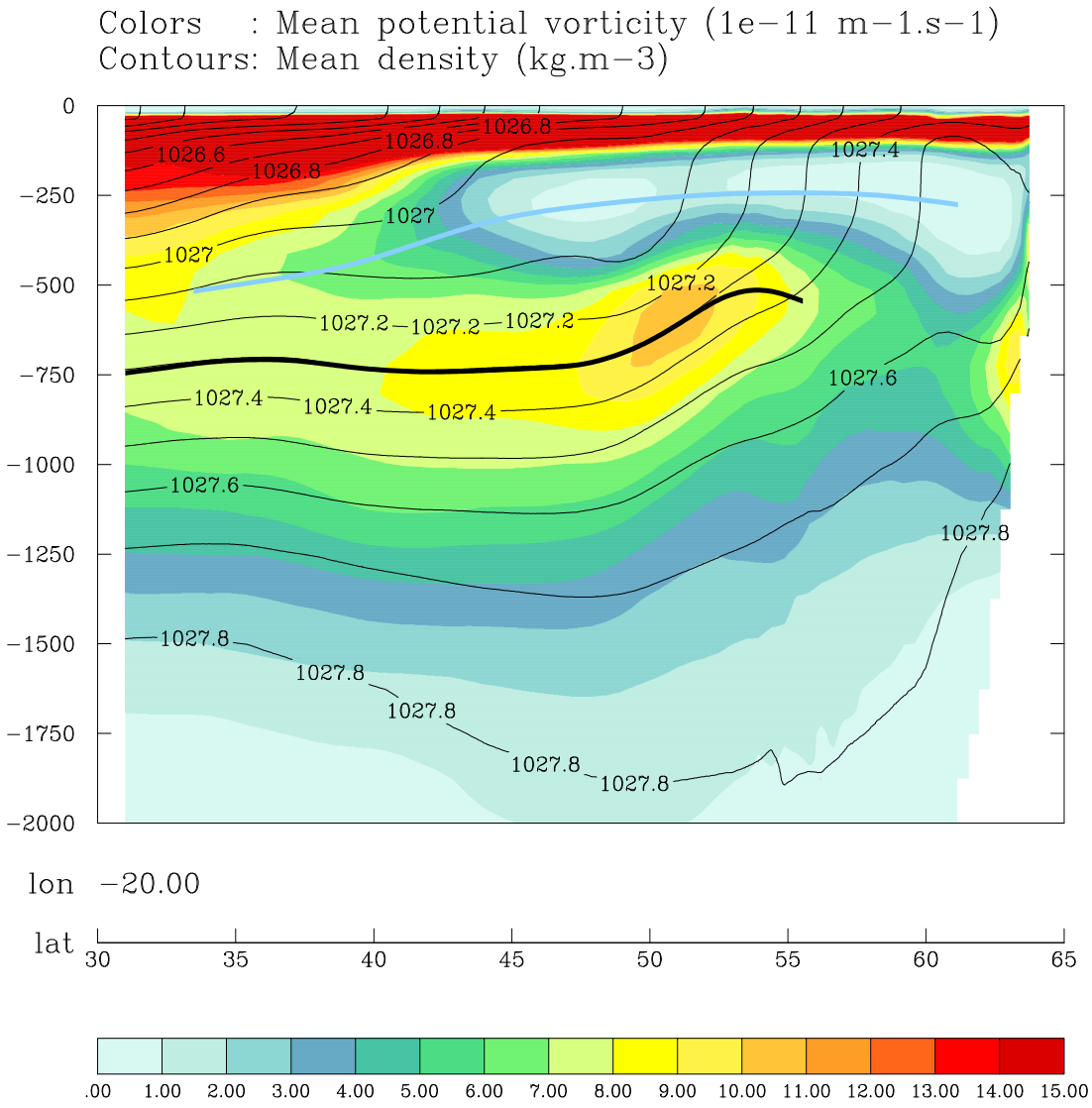
Colors : Mean potential vorticity (1e−11 m−1.s−1)
Contours: Mean density (kg.m−3)
0
−250
−500
−750
−1000
−1250
−1500
−1750
−2000
1026.6
1026.8
1026.8
1026.8
1027
1027
1027.2
1027.2
1027.2
1027.2
1027.4
1027.4
1027.4
1027.4
1027.6
1027.6
1027.8
1027.8
1027.8
1027.8
1027.8
1027.8
lon −20.00
lat
30
35
40
45
50
55
60
65
.00
1.00
2.00
3.00
4.00
5.00
6.00
7.00
8.00
9.00
10.00
11.00
12.00
13.00
14.00
15.00

Figure 7

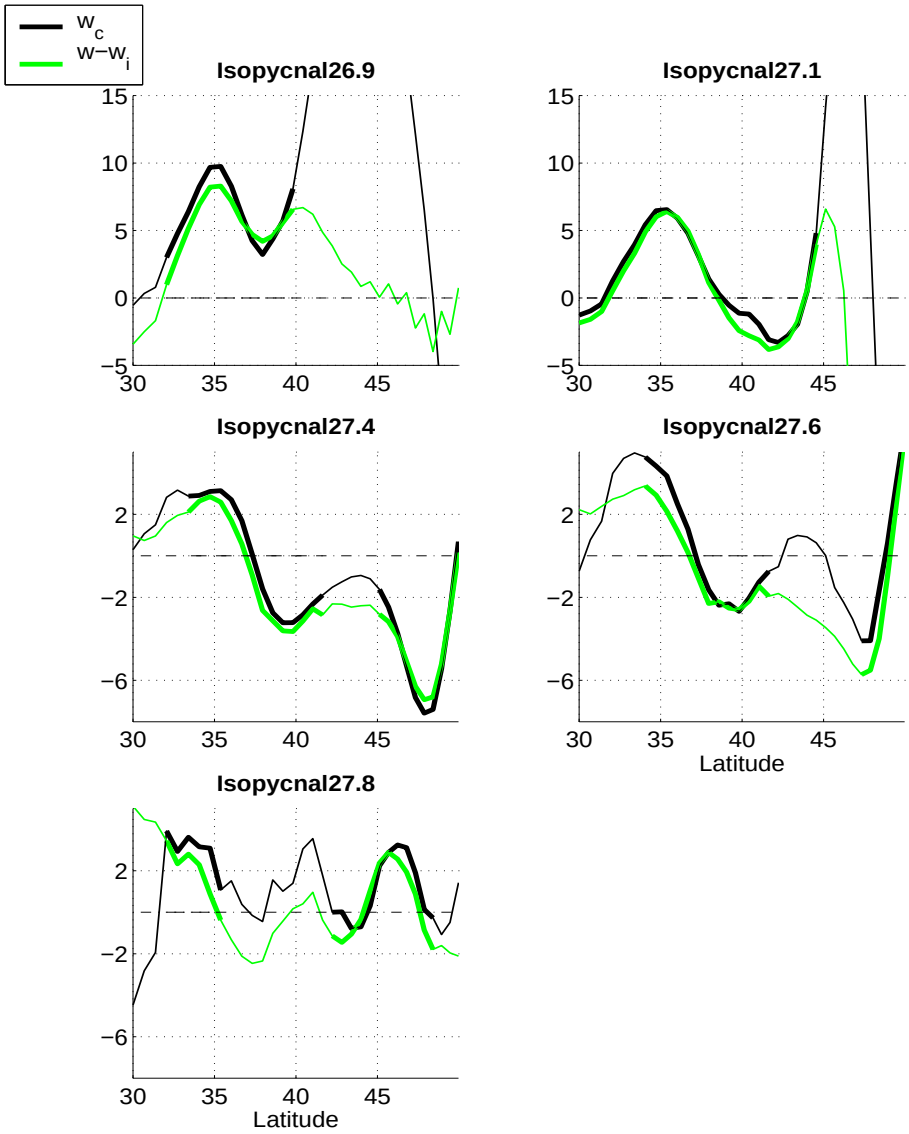
w_c
w−w_i
Isopycnal26.9
Isopycnal27.1
Isopycnal27.4
Isopycnal27.6
Isopycnal27.8
Latitude
Latitude

Figure 8

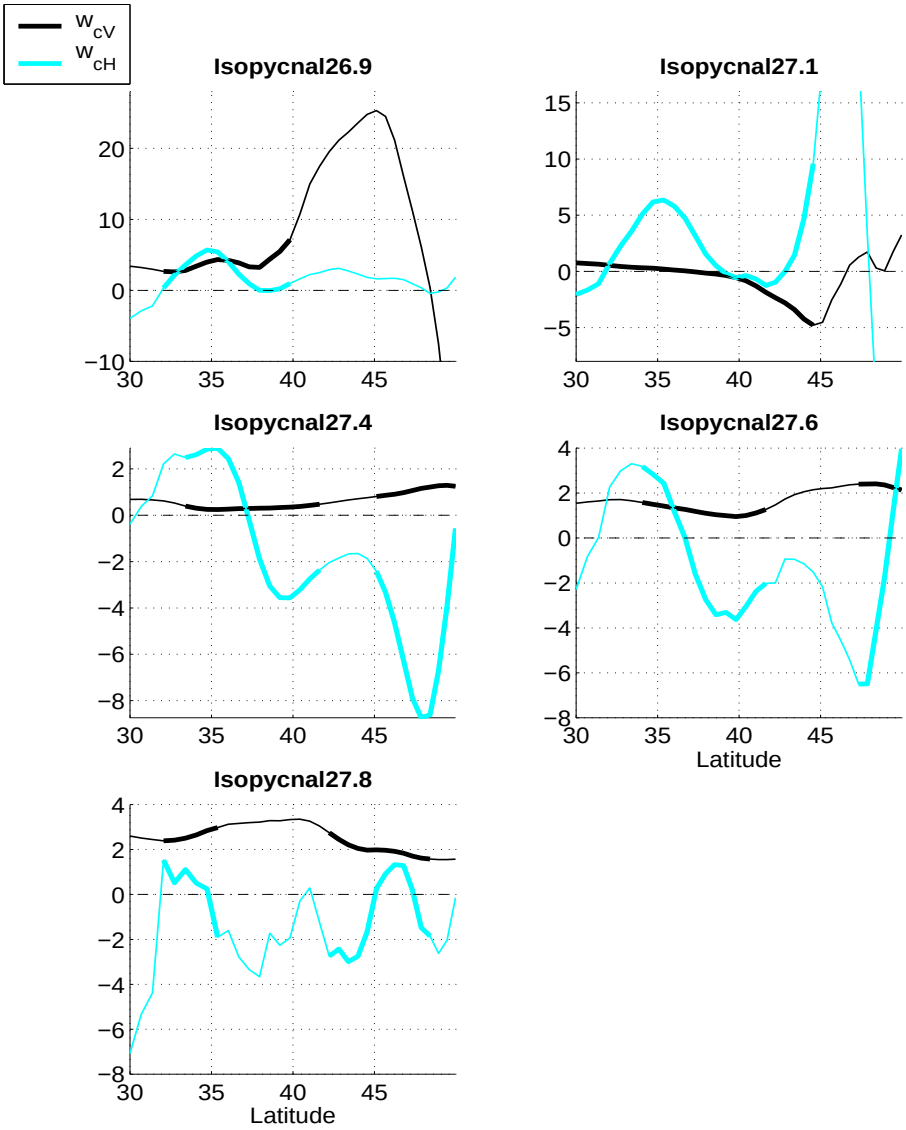
w_cV
w_cH
Isopycnal26.9
Isopycnal27.1
Isopycnal27.4
Isopycnal27.6
Isopycnal27.8
Latitude
Latitude

Figure 9

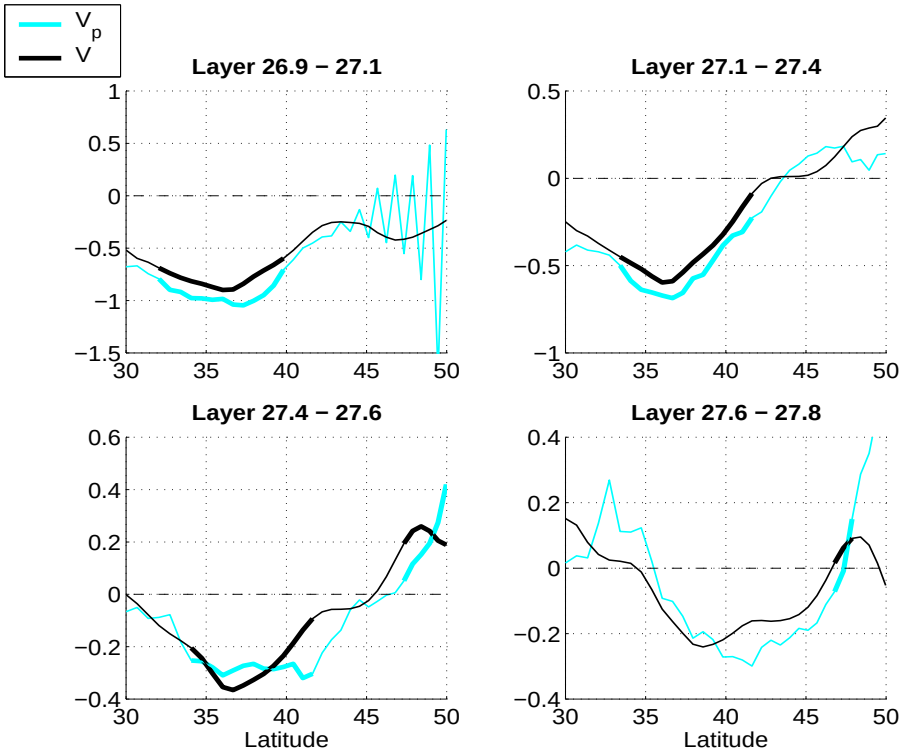
V_p
V
Layer 26.9 − 27.1
Layer 27.1 − 27.4
Layer 27.4 − 27.6
Layer 27.6 − 27.8
Latitude
Latitude

Figure 10

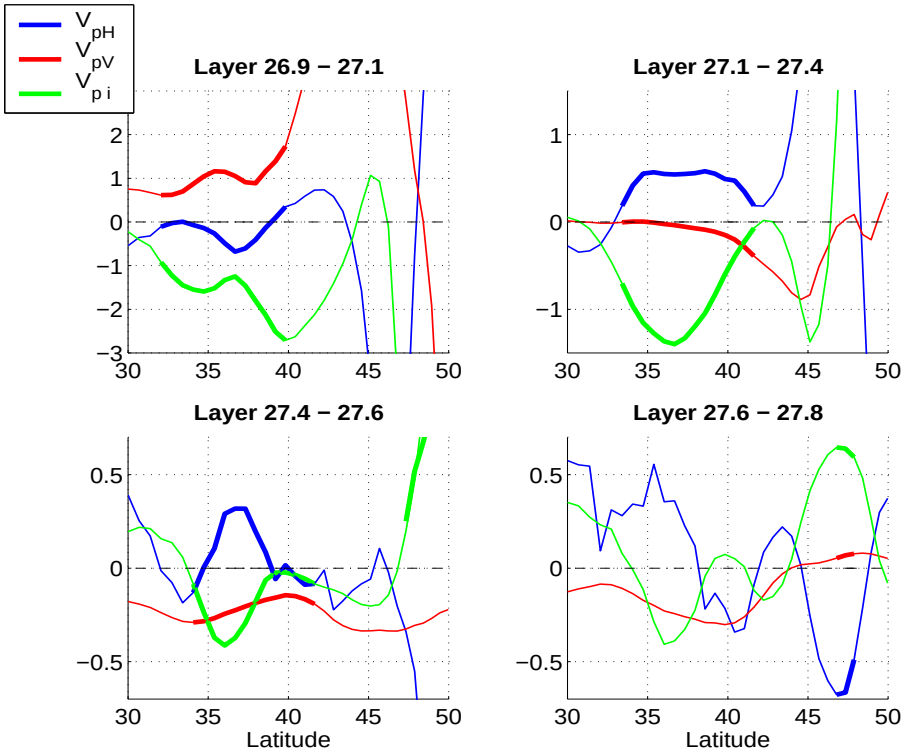
V pH
V pV
V p i
Layer 26.9 − 27.1
Layer 27.1 − 27.4
Layer 27.4 − 27.6
Layer 27.6 − 27.8
Latitude
Latitude

Figure 11